# Electron-impact ionization of helium: A comprehensive experiment benchmarks theory

X. Ren,[1] I. Bray,[2] D.V. Fursa,[2] J. Colgan,[3] M.S. Pindzola,[4] T. Pflüger,[1] A. Senftleben,[1] S. Xu,[1] A. Dorn,[1,*] and J. Ullrich[1]

[1]*Max-Planck-Institute for Nuclear Physics, DE-69117 Heidelberg, Germany*

[2]*ARC Centre for Antimatter-Matter Studies, Curtin University, GPO Box U1987 Perth, Western Australia, Australia*

[3]*Theoretical Division, Los Alamos National Laboratory, Los Alamos, New Mexico 87545, USA*

[4]*Department of Physics, Auburn University, Auburn, Alabama 36849, USA*

(Received 15 February 2011; published 24 May 2011)

Single ionization of helium by 70.6-eV electron impact is studied in a comprehensive experiment covering a major part of the entire collision kinematics and the full $4\pi$ solid angle for the emitted electron. The absolutely normalized triple-differential experimental cross sections are compared with results from the convergent close-coupling (CCC) and the time-dependent close-coupling (TDCC) theories. Whereas excellent agreement with the TDCC prediction is only found for equal energy sharing, the CCC calculations are in excellent agreement with essentially all experimentally observed dynamical features, including the absolute magnitude of the cross sections.

DOI: 10.1103/PhysRevA.83.052711 PACS number(s): 34.80.Dp

## I. INTRODUCTION

Collisions of electrons with atoms and molecules that drive chemical and physical reactions are of utmost importance for a broad range of areas from plasma physics to radiation damage in living tissue or the chemistry in planetary atmospheres. Moreover, they are of basic intrinsic interest since they constitute one of the most fundamental realizations of the ubiquitous correlated quantum-dynamical few-body problem. Kinematically complete experiments for electron-impact single ionization of atoms, so-called $(e,2e)$ studies, determine the momentum vectors of all continuum particles for known final-state configuration of the remaining ion, thus ultimately benchmarking all facets of quantum few-body Coulomb dynamics.

Electron-impact-induced single ionization is a breakup reaction with three free charged particles in the final channel interacting via long-range Coulomb forces posing enormous challenges to theory. The complete description of this problem requires covering all possible sets of the kinematical parameters for any initial- and final-state electron energies $\boldsymbol{E}_0$, $\boldsymbol{E}_1$, $\boldsymbol{E}_2$, as well as momenta $\vec{k}_0$, $\vec{k}_1$ ,$\vec{k}_2$ , thus calling for approaches that go beyond perturbation theory. So far, only the most fundamental three-particle quantum-dynamical problem, electron-impact ionization of atomic hydrogen, was claimed, having been rigorously solved numerically by *ab initio* methods. These are (i) the exterior complex scaling (ECS) [1], (ii) the time-dependent close-coupling (TDCC) [2], and (iii) the convergent close-coupling (CCC) [3] theories. Just going to helium, however, with only one additional bound electron, the full correlated four-particle problem can not be solved without approximations such that it represents an ideal target to study few-body quantum dynamics beyond three particles. Therefore, it has been extensively studied experimentally for impact energies from close to threshold up to 8 keV (see, e.g., [4,10]). Theoretically, the structure of the helium atom is dominated by one-electron excitations, which allow for a quite accurate description. The nonperturbative CCC and TDCC methods have been successfully applied to describe electron-helium ionizing collisions yielding, in general, excellent agreement with all available experimental data (see, e.g., [5,11,15],). Thus, recently the question was posed by Bray *et al.* [13] as to whether the problem of single ionization of helium by electron impact, leaving the ion in the ground state, has also been computationally solved. However, puzzling systematic discrepancies observed for some of the coplanar data question this statement, calling for comprehensive measurements to benchmark theory. To this end, experimental data are required that are normalized to an absolute scale for any final-state continuum covering a broad range of collision kinematics, coplanar as well as out of plane, and a large part of the $4\pi$ solid angle of electron emission.

In this paper, we comprehensively explore single ionization of helium by 70.6-eV electron impact. Absolute fully differential cross sections are reported, covering a major part of the three-particle final-state via three-dimensional (3D) $(e,2e)$ cross sections ranging from equal to unequal energy sharing between both outgoing electrons, different sets of projectile scattering angles, as well as "in-plane" and "out-of-plane" geometries.

## II. EXPERIMENT

The experiments were performed using an advanced reaction microscope [16], which is especially designed for electron collision experiments. The setup was described before [8,17], and only a brief outline will be given here. A well-focused (1 mm diameter), pulsed electron beam (pulse width $\approx$1.5 ns), produced by a standard thermocathode gun, intersects a cold helium gas jet (2 mm diameter) created by supersonic expansion. By using parallel electric and magnetic fields, both the final-state electrons and the recoiling ion are projected onto two-dimensional position- and time-sensitive detectors in opposite directions. From the positions of the hits and the times of flight, the initial momentum vectors of the detected fragments can be determined. A large part of the entire $4\pi$ solid angle is covered for the final-state particles, 100% for the detection of the recoil ion, and about 80% for electrons. Electrons miss the detector for energies transversal to the

*Alexander.Dorn@mpi-hd.mpg.de

 

spectrometer axis higher than 15 eV and for particular times of flight where they arrive close to the spectrometer axis in a bore hole in the electron detector, which is required for the passage of the projectile beam. Experiments for unequal energy sharing ($\boldsymbol{E}_2 \leqslant 15$ eV) were obtained through triple-coincidence detection between two outgoing electrons ($e_1$ and $e_2$) and the recoiling ion. The momentum vectors $\vec{k}_1$ and $\vec{k}_2$ are measured directly, and the recoil-ion momentum ($\vec{k}_r$) is used as a reference signal for calibration and efficiently subtracting the background as discussed in [17,18]. For the equal energy sharing case ($\boldsymbol{E}_1 = \boldsymbol{E}_2 = 23$ eV), experimental data were obtained from double-coincidence events between one of the outgoing electrons ($\vec{k}_1$) and the recoil ion ($\vec{k}_r$). The momentum ($\vec{k}_2$) of the second electron is then calculated by applying momentum conservation as discussed in [5]. The absolute scale of the cross section was obtained by normalizing to the absolute measurements in coplanar geometry by Röder *et al.* as reported in [19]. All data in the present experiment were recorded simultaneously in a single run. Consequently, once the normalization factor has been fixed for one point, the cross sections for all the other geometries are automatically normalized with respect to each other for all recorded scattering angles and all ejected electron energies. See Tables I–III for the experimental absolute TDCS values.

## III. RESULTS AND DISCUSSIONS

The details of theoretical approaches to differential ionization have already been extensively discussed in [14,15] for CCC and in [11,12] for TDCC. The calculations presented here have the same foundation as described by Bray *et al.* [13] for CCC and by Colgan *et al.* [12] for TDCC, suitably modified for the present kinematics and geometries. Triple-differential cross sections (TDCS) as 3D emission patterns for experiment and CCC calculation are presented in Figs. 1(a) and 1(b), respectively, for the scattering angle of $\boldsymbol{\theta}_1 = -20^\circ$ of the fast final-state electron as a function of the emission direction of a slow ejected electron with $\boldsymbol{E}_2 = 5$ eV energy. The projectile is coming in from the bottom ($\vec{k}_0$) and scattered to the left ($\vec{k}_1$). (We count positive angles from the projectile forward direction clockwise.) These two vectors define the scattering plane as indicated by the dashed frame in Fig. 1(a). The TDCS for a particular direction is given by the distance from the origin of the plot (also corresponding to the collision point) to the point on the surface, which is intersected by the ionized electron's emission direction. The kinematics chosen displays the principal features of the cross-section pattern. It is governed by the well-known binary and recoil lobes that are aligned roughly along and opposite the indicated momentum transfer vector $\vec{q}$, respectively. Both lobes are bent backwards since

TABLE I. Experimental absolute TDCS in the scattering (||) and perpendicular (⊥) plane as a function of the emission angle ($\theta_2$) of an electron with $E_2 = 5$ eV. The scattering angle ($\theta_1$) is varied from $-10^\circ$ to $-30^\circ$. The TDCS are in units of $10^{-21}$ cm$^2$ sr$^{-2}$ eV$^{-1}$.

| | $\theta_1 = -10^\circ$ | | $\theta_1 = -15^\circ$ | | $\theta_1 = -20^\circ$ | | $\theta_1 = -25^\circ$ | | $\theta_1 = -30^\circ$ | |
|---|---|---|---|---|---|---|---|---|---|---|
| $\theta_2(^\circ)$ | \|\| | ⊥ | \|\| | ⊥ | \|\| | ⊥ | \|\| | ⊥ | \|\| | ⊥ |
| 25 | 101.8 | 46.1 | 44.5 | 21.8 | 25.5 | 10.7 | | | | |
| 35 | 178.6 | 69.1 | 87.2 | 33.6 | 41.5 | 17.9 | 25.3 | 11.2 | 20.8 | 13.7 |
| 45 | 287.3 | 80.5 | 203.2 | 55.5 | 95.7 | 27.3 | 50.2 | 21.8 | 28.2 | 14.6 |
| 55 | 381.6 | 116.6 | 264.2 | 68.2 | 190.2 | 46.7 | 97.8 | 27.1 | 51.8 | 19.7 |
| 65 | 461.3 | 130.0 | 368.5 | 93.5 | 231.5 | 54.0 | 135.3 | 35.8 | 71.0 | 24.5 |
| 75 | 435.0 | 115.0 | 384.5 | 84.5 | 245.8 | 54.2 | 154.2 | 38.8 | 84.4 | 27.3 |
| 85 | 309.0 | 86.0 | 291.8 | 81.8 | 212.6 | 49.8 | 137.0 | 37.3 | 80.2 | 23.9 |
| 95 | 217.0 | 97.0 | 226.8 | 95.5 | 168.8 | 57.7 | 123.0 | 32.7 | 69.7 | 21.2 |
| 105 | 99.0 | 132.0 | 73.8 | 71.3 | 65.9 | 48.9 | 47.6 | 23.5 | 29.8 | 15.1 |
| 115 | 68.0 | 205.6 | 48.7 | 114.9 | 34.2 | 73.5 | 21.8 | 33.0 | 17.1 | 16.0 |
| 125 | 95.0 | 345.0 | 59.7 | 170.2 | 22.8 | 87.9 | 12.0 | 39.7 | 8.7 | 20.6 |
| 135 | 177.6 | 354.0 | 65.3 | 193.6 | 29.8 | 109.0 | 15.8 | 53.4 | 7.9 | 27.5 |
| 145 | 235.0 | 444.0 | 110.5 | 261.4 | 43.0 | 130.2 | 20.3 | 57.8 | 8.4 | 30.5 |
| 155 | 335.0 | 598.9 | 153.2 | 266.1 | 77.5 | 155.7 | 43.6 | 82.6 | 16.7 | 37.2 |
| 205 | 796.1 | 587.3 | 427.6 | 294.8 | 221.0 | 165.5 | 119.0 | 87.3 | 60.6 | 41.4 |
| 215 | 779.0 | 451.0 | 418.6 | 306.8 | 225.9 | 136.5 | 116.4 | 72.5 | 57.1 | 36.5 |
| 225 | 652.8 | 403.0 | 393.2 | 232.3 | 212.5 | 126.5 | 110.3 | 55.1 | 51.5 | 29.4 |
| 235 | 592.0 | 312.0 | 364.5 | 156.7 | 201.8 | 68.9 | 92.1 | 34.9 | 48.2 | 23.8 |
| 245 | 504.8 | 222.4 | 311.8 | 122.8 | 184.2 | 85.0 | 77.5 | 40.4 | 39.8 | 24.5 |
| 255 | 374.0 | 151.0 | 220.4 | 90.5 | 128.2 | 53.6 | 57.9 | 32.9 | 31.8 | 17.5 |
| 265 | 259.0 | 102.0 | 165.9 | 102.3 | 106.0 | 65.1 | 51.3 | 38.0 | 26.1 | 22.8 |
| 275 | 141.0 | 104.0 | 112.7 | 88.2 | 67.4 | 56.3 | 42.5 | 36.0 | 23.0 | 27.1 |
| 285 | 89.0 | 103.0 | 89.1 | 93.6 | 52.1 | 59.3 | 30.7 | 36.8 | 17.1 | 23.2 |
| 295 | 66.3 | 131.3 | 58.9 | 114.5 | 36.3 | 49.6 | 21.8 | 34.5 | 11.2 | 27.4 |
| 305 | 32.9 | 105.8 | 37.3 | 69.6 | 21.7 | 46.6 | 18.2 | 26.5 | 8.3 | 17.8 |
| 315 | 19.4 | 82.9 | 16.5 | 53.5 | 12.6 | 27.7 | 7.5 | 14.9 | 4.0 | 9.3 |
| 325 | 28.8 | 84.5 | 8.0 | 32.8 | 5.8 | 18.3 | 3.5 | 7.7 | 4.9 | 12.5 |
| 335 | 26.9 | 51.8 | 9.6 | 27.9 | 2.7 | 5.8 | | | | |

TABLE II. Experimental absolute TDCS in the scattering (||) and perpendicular (⊥) plane as a function of the ejected electron emission angle ($\theta_2$) for two ejected electron energies of $E_2 = 3$ and 10 eV and two scattering angles of $\theta_1 = -10^\circ$ and $-30^\circ$. The TDCS are in units of $10^{-21}$ cm$^2$ sr$^{-2}$ eV$^{-1}$.

| | $\theta_1 = -10^\circ$, $E_2$= 3eV | | $\theta_1 = -10^\circ$, $E_2 = 10$eV | | $\theta_1 = -30^\circ$, $E_2 = 3$eV | | $\theta_1 = -30^\circ$, $E_2 = 10$eV | |
|---|---|---|---|---|---|---|---|---|
| $\theta_2(^\circ)$ | \|\| | ⊥ | \|\| | ⊥ | \|\| | ⊥ | \|\| | ⊥ |
| 35 | 157.1 | 52.4 | 73.5 | 25.3 | | | 19.3 | 6.3 |
| 45 | 265.7 | 77.2 | 149.9 | 40.8 | 22.7 | 12.9 | 45.3 | 11.4 |
| 55 | 450.0 | 148.0 | 215.7 | 56.7 | 43.0 | 18.9 | 65.5 | 17.5 |
| 65 | 570.9 | 163.6 | 252.2 | 67.3 | 57.4 | 19.8 | 88.6 | 20.8 |
| 75 | 519.3 | 137.5 | 215.5 | 48.4 | 69.3 | 21.8 | 90.3 | 26.5 |
| 85 | 463.6 | 89.1 | 153.0 | 55.6 | 69.9 | 23.8 | 77.3 | 25.0 |
| 95 | 379.6 | 91.6 | 83.5 | 46.4 | 60.2 | 17.2 | 54.3 | 23.6 |
| 105 | 129.1 | 125.5 | 52.8 | 73.9 | 32.6 | 14.6 | 27.0 | 20.6 |
| 115 | 82.9 | 235.6 | 58.1 | 121.7 | 22.9 | 17.4 | 10.6 | 19.2 |
| 125 | 109.1 | 463.6 | 85.5 | 136.8 | 13.3 | 23.0 | 7.6 | 17.8 |
| 135 | 260.9 | 551.1 | 141.0 | 153.2 | 9.4 | 26.1 | 9.3 | 27.3 |
| 145 | | | 196.5 | 226.3 | | | 14.8 | 33.6 |
| 155 | | | 243.5 | 236.1 | | | 18.5 | 35.1 |
| 205 | | | 362.5 | 236.9 | | | 46.9 | 31.5 |
| 215 | | | 335.3 | 211.7 | | | 45.4 | 31.3 |
| 225 | 971.8 | 545.9 | 281.0 | 156.0 | 67.2 | 30.6 | 40.8 | 27.6 |
| 235 | 950.9 | 456.4 | 235.5 | 122.0 | 64.1 | 25.6 | 37.5 | 22.4 |
| 245 | 746.2 | 276.4 | 220.1 | 112.0 | 48.0 | 20.7 | 33.1 | 25.3 |
| 255 | 392.7 | 165.5 | 169.2 | 78.4 | 32.6 | 19.4 | 30.6 | 26.3 |
| 265 | 315.8 | 111.3 | 96.5 | 64.4 | 27.8 | 20.8 | 23.6 | 22.8 |
| 275 | 220.0 | 127.3 | 85.0 | 52.8 | 22.8 | 21.6 | 19.0 | 29.2 |
| 285 | 154.9 | 106.9 | 41.0 | 57.2 | 15.1 | 19.0 | 11.2 | 27.0 |
| 295 | 89.1 | 174.5 | 38.4 | 67.6 | 15.2 | 20.7 | 6.2 | 24.9 |
| 305 | 68.0 | 148.0 | 28.6 | 42.4 | 9.6 | 20.6 | 5.9 | 17.4 |
| 315 | 28.8 | 87.7 | 16.9 | 38.2 | 4.5 | 9.4 | 4.4 | 13.1 |
| 325 | 20.9 | 52.4 | 13.4 | 28.2 | | | 1.7 | 7.3 |

the emitted electron is repelled by the scattered projectile due to the long-range nature of the Coulomb force. The strength of this post-collision interaction (PCI) effect increases with decreasing relative energy of the two outgoing electrons, and it clearly becomes relevant at the present low-impact energy. Another striking feature in the 3D patterns is the significant cross section outside of the scattering plane filling up the angular range in-between the binary and recoil lobes. This was first observed for ion-impact single ionization of helium [20], where it is still not fully understood. Figure 1 exhibits excellent agreement of the experimental and the CCC results. The qualitative features observed in the experiment are very well reproduced by this theoretical method.

For quantitative comparisons of experiment and the CCC and TDCC theories, Figs. 2(a) and 2(b) present the TDCS in the scattering plane (the dashed frame in Fig. 1) and the so-called perpendicular plane, which is perpendicular to the scattering plane and includes the incoming projectile beam (the dotted frame in Fig. 1), respectively. Also presented in Fig. 2 are the TDCS in the scattering and perpendicular planes for different scattering angles from $\boldsymbol{\theta}_1 = -10^\circ$ to $-30^\circ$ and the same ejection energy of $\boldsymbol{E}_2 = 5$ eV. The TDCS in the scattering plane (left column) clearly show the basic features of binary (peaked at $\boldsymbol{\theta}_2 \sim 75^\circ$) and recoil lobes (peaked at $\boldsymbol{\theta}_2 \sim 210^\circ$). In the perpendicular plane (right column), three peaks are observed, one strong peak at $\boldsymbol{\theta}_2 = 180^\circ$ (peak I), and two side peaks at $\boldsymbol{\theta}_2 \sim 60^\circ$ and $300^\circ$ (peaks II). The insets in Figs. 2(c)–2(j) are the 3D patterns of TDCS for experiment (left column) and CCC theory (right column). Excellent agreement between experimental data and CCC calculations are found for both in and out of the scattering plane and the 3D patterns. In contrast, discrepancies are observed in comparison with the TDCC theory, where the magnitude of the cross section at the recoil region is significantly higher than in the experiment. From lower ($\boldsymbol{\theta}_1 = -10^\circ$) to higher ($\boldsymbol{\theta}_1 = -30^\circ$) scattering angles, the absolute magnitude of the TDCS decreases strongly and the binary-to-recoil ratio in the scattering plane increases. In the perpendicular plane, the peak-II-to-peak-I ratio also grows. As we can see from the 3D pattern in Fig. 1(a), the perpendicular plane cuts through the recoil lobe of the 3D pattern in the backward direction. Therefore, the origin of peak I is the well-known nuclear backscattering process leading to the recoil lobe [6]. The peaks II, however, are attributed to the significant contribution of higher-order processes filling up the region in-between the binary and recoil lobes as discussed in [18], [21]. All the features observed in the experiment are fully reproduced by the CCC theory, and show excellent accuracy in the absolute magnitude. The experimental absolute TDCS values of the above discussed ($e$,2$e$) kinematics are shown in Table I.

Further quantitative comparisons between experiment and the theories are shown in Fig. 3, where the cross sections for $\boldsymbol{\theta}_1 = -10^\circ$ and $-30^\circ$ and $\boldsymbol{E}_2 = 3$ and 10 eV are

TABLE III. Experimental absolute TDCS in the scattering (||) and perpendicular (⊥) plane for equal energy sharing ($E_1 = E_2 = 23$ eV) as a function of electron emission angle ($\theta_2$) at different scattering angles $\theta_1 = -30°$, $-60°$, and $-120°$. The TDCS are in units of $10^{-21}$ cm$^2$ sr$^{-2}$ eV$^{-1}$.

| | $\theta_1 = -30°$ | | $\theta_1 = -60°$ | | $\theta_1 = -120°$ | |
|---|---|---|---|---|---|---|
| $\theta_2$(°) | \|\| | ⊥ | \|\| | ⊥ | \|\| | ⊥ |
| 5 | 4.6 | 3.7 | 42.7 | 32.8 | 39.0 | 40.3 |
| 15 | 5.8 | 3.2 | 55.1 | 25.2 | 32.0 | 37.0 |
| 25 | 19.7 | 4.2 | 54.8 | 16.5 | 12.8 | 21.1 |
| 35 | 22.2 | 4.2 | 32.8 | 10.9 | 4.0 | 10.0 |
| 45 | 42.8 | 6.3 | 16.6 | 5.4 | 2.4 | 4.5 |
| 55 | 54.2 | 9.4 | 9.6 | 4.9 | 1.9 | 2.5 |
| 65 | 52.9 | 11.8 | 6.3 | 4.3 | 1.8 | 1.3 |
| 75 | 35.8 | 13.1 | 4.2 | 3.8 | 2.1 | 1.1 |
| 85 | 24.0 | 9.7 | 2.1 | 2.8 | 1.8 | 0.5 |
| 95 | 13.4 | 11.5 | 1.6 | 2.4 | 1.0 | 0.5 |
| 105 | 6.9 | 10.0 | 1.2 | 2.6 | 1.8 | 0.4 |
| 115 | 9.8 | 10.8 | 1.2 | 2.4 | 1.8 | 0.5 |
| 125 | 9.5 | 13.7 | 2.3 | 2.7 | 1.4 | 0.1 |
| 135 | 13.1 | 15.7 | 2.7 | 3.2 | 1.8 | 0.5 |
| 145 | 18.2 | 16.7 | 4.3 | 5.4 | 1.9 | 0.3 |
| 155 | 15.3 | 17.7 | 8.3 | 6.7 | 1.3 | 0.6 |
| 165 | 18.0 | 23.1 | 9.2 | 7.2 | 1.3 | 0.6 |
| 175 | 17.9 | 20.1 | 8.7 | 8.4 | 0.8 | 0.3 |
| 185 | 21.0 | 17.9 | 7.3 | 7.6 | 0.1 | 0.6 |
| 195 | 21.2 | 17.7 | 6.7 | 7.7 | 0.0 | 0.5 |
| 205 | 19.8 | 14.8 | 3.2 | 6.2 | 0.0 | 0.6 |
| 215 | 15.9 | 15.4 | 1.8 | 5.5 | 0.0 | 0.6 |
| 225 | 14.9 | 12.5 | 1.1 | 3.4 | 0.1 | 0.6 |
| 235 | 13.5 | 13.5 | 0.7 | 2.8 | 0.0 | 0.5 |
| 245 | 8.6 | 10.5 | 0.2 | 2.1 | 0.0 | 0.5 |
| 255 | 7.2 | 9.7 | 0.1 | 2.3 | 0.0 | 0.6 |
| 265 | 6.0 | 11.5 | 0.0 | 1.9 | 0.1 | 0.8 |
| 275 | 6.6 | 13.8 | 0.0 | 3.1 | 0.0 | 1.0 |
| 285 | 2.3 | 14.6 | 0.0 | 3.8 | 0.3 | 2.0 |
| 295 | 1.4 | 14.5 | 0.0 | 4.8 | 0.3 | 2.1 |
| 305 | 0.3 | 13.4 | 0.0 | 6.0 | 2.1 | 2.6 |
| 315 | 0.2 | 10.8 | 0.1 | 7.8 | 3.8 | 3.9 |
| 325 | 0.0 | 5.6 | 0.6 | 11.6 | 9.0 | 6.4 |
| 335 | 0.5 | 7.1 | 3.0 | 16.8 | 21.1 | 15.8 |
| 345 | 1.8 | 4.2 | 8.2 | 22.1 | 32.9 | 25.1 |
| 355 | 2.3 | 3.5 | 22.2 | 31.4 | 40.0 | 40.4 |

presented in the scattering plane (left column) and perpendicular plane (right column). Also included in Figs. 3(a)–3(h) are the 3D TDCS patterns for experiment (left column) and CCC theory (right column). The basic features of the TDCS in the scattering, perpendicular planes, and 3D images are quite similar to that discussed above. Agreement between experiment and CCC prediction is again excellent, confirming that the CCC calculation is sufficiently accurate to reproduce all the experimental observations. Again, the TDCC calculations tend to overestimate the cross section in the recoil region, especially for $\boldsymbol{E}_2 = 3$ eV ejection energy. The experimental absolute TDCS values of the above discussed (*e*,2*e*) kinematics are shown in Table II.

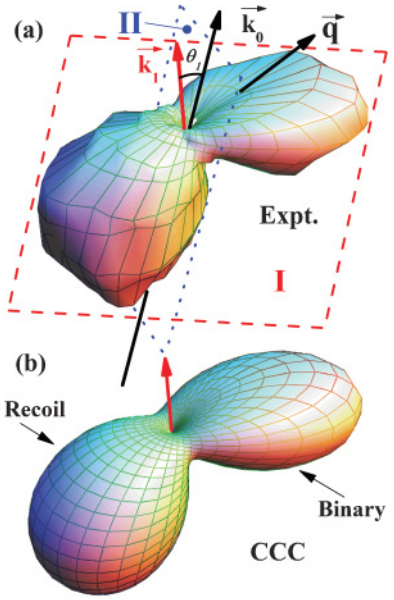


FIG. 1. (Color online) Absolute TDCS for (*e*,2*e*) on He as a function of the emission angle of an electron with kinetic energy of $E_2 = 5$ eV. The emission angle of the other electron ($E_1 = 41$ eV) is fixed to $\theta_1 = -20°$. (a) Experimental 3D cross section. (b) CCC calculation. The dashed and dotted frames in (a) indicate the cutting planes through 3D pattern in the scattering (I) and perpendicular plane (II), respectively.

A comparison at equal energy sharing ($\boldsymbol{E}_1 = \boldsymbol{E}_2 = 23$ eV) is provided in Fig. 4, where the cross sections in the scattering and perpendicular planes are shown in the left and right columns, respectively, and also the 3D patterns are presented for experiment (left column) and CCC calculations (right column). The results at $\boldsymbol{\theta}_1 = -30°$ scattering angle show again the basic binary and recoil peaks in the scattering plane and three peaks in the perpendicular plane. Moving to $\boldsymbol{\theta}_1 = -60°$ and $-120°$, the binary-to-recoil ratio is increasing strongly. The binary and recoil peaks are shifted toward the direction of $\boldsymbol{\theta}_2 = 0°$, and two side peaks in the perpendicular plane merge to one strong maximum at $\boldsymbol{\theta}_2$ around 0°. In comparison with theory, this equal energy sharing case is the only one where distinct deviations of the CCC result can be found. These are the binary peak magnitude in Fig. 4(c) as well as the recoil peak heights in 4(d) and 4(e). These discrepancies do not seem to follow a systematic trend. On the other hand, different from the asymmetric energy sharing cases, the TDCC results here are in good agreement and even surpass the accuracy of the CCC result. Examples are the magnitudes of the binary peak in Fig. 4(c) and the recoil peak in Fig. 4(e).

In order to judge the accuracy of the experimental data, it should be noted that the statistical errors are given by the error bars of the data points. Possible systematic errors are hard to quantify, but one can get an idea of their importance considering that the TDCS in the perpendicular plane must be mirror symmetric with respect to $\boldsymbol{\theta}_2 = 180°$. This symmetry is fulfilled in all cases except in Fig. 4(d), where the FDCS between 30° and 60° shows some deviation from the respective data between 300° and 330°. The experimental absolute TDCS

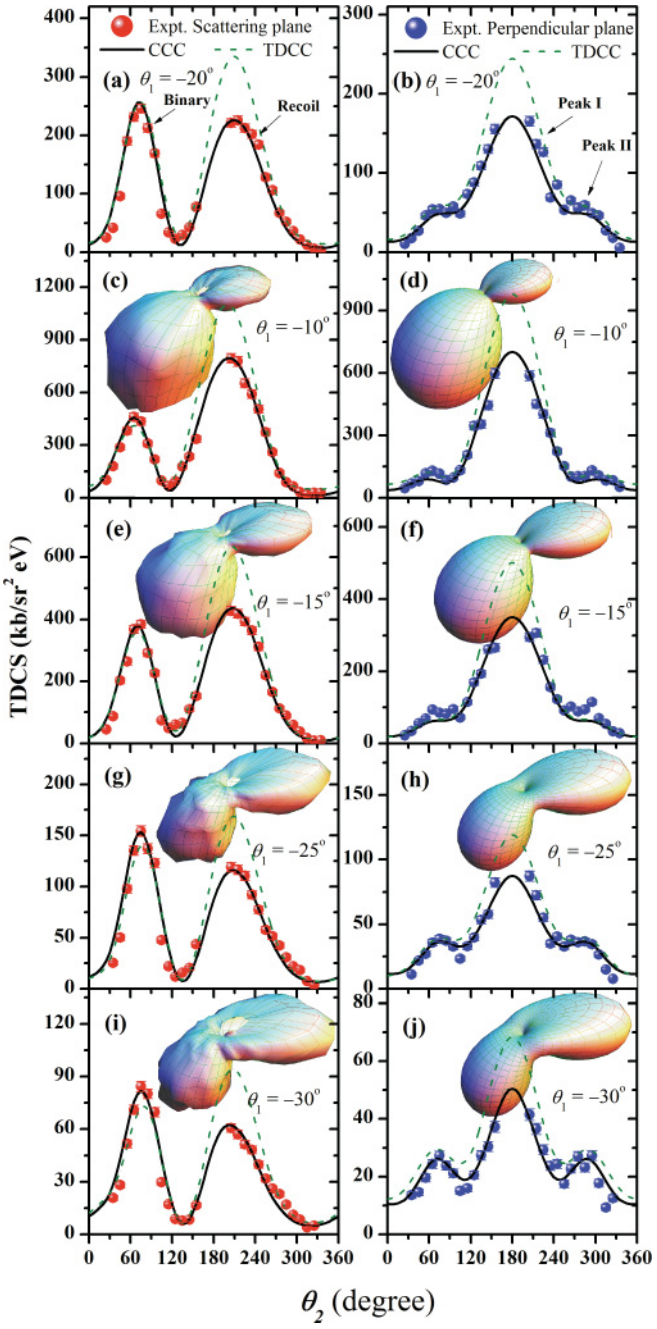


FIG. 2. (Color online) Absolute TDCS in the scattering (left column) and perpendicular plane (right column) as a function of the emission angle of an electron with $E_2 = 5$ eV. The other electron's ($E_1 = 41$ eV) emission angle $\theta_1$ is fixed to (a) and (b) $\theta_1 = -20°$; (c) and (d) $\theta_1 = -10°$; (e) and (f) $\theta_1 = -15°$; (g) and (h) $\theta_1 = -25°$; (i) and (j) $\theta_1 = -30°$. The insets in (c)– (j) are the 3D patterns of the TDCS for experiment (left column) and CCC calculation (right column).

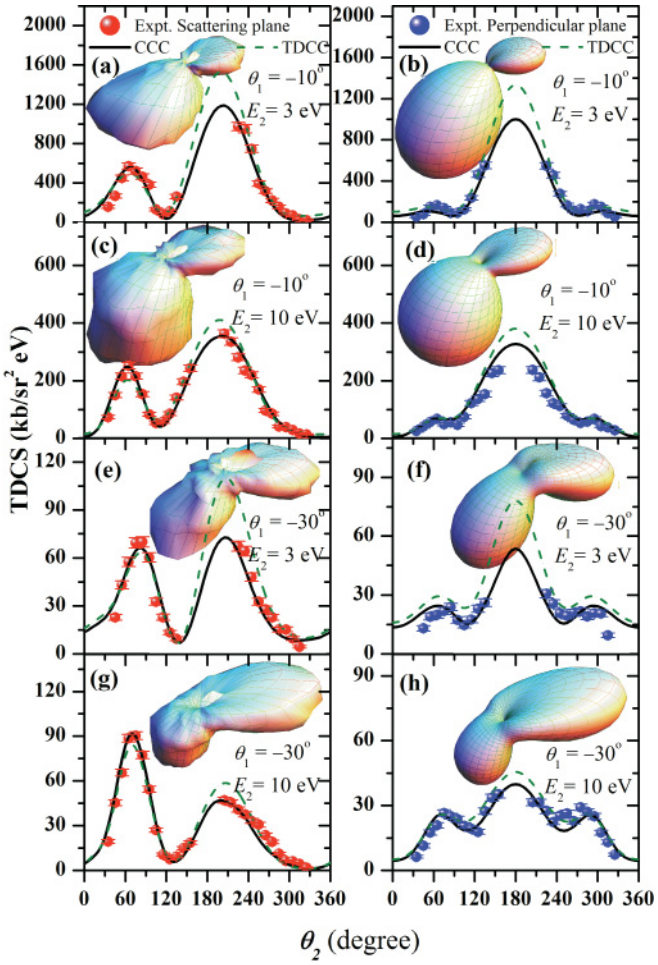


FIG. 3. (Color online) Absolute TDCS in the scattering (left column) and perpendicular plane (right column) as a function of the emission angle $\theta_2$ of one electron with energy $E_2$. The other electron's emission angle $\theta_1$ is fixed: (a) and (b) $\theta_1 = -10°$, $E_2 = 3$ eV ; (c) and (d) $\theta_1 = -10°$, $E_2 = 10$ eV; (e) and (f) $\theta_1 = -30°$, $E_2 = 3$ eV; (g) and (h) $\theta_1 = -30°$, $E_2 = 10$ eV. The insets in (a)–(h) are the 3D patterns of the TDCS for the experiment (left column) and CCC calculation (right column).

values of the above discussed equal energy sharing conditions are shown in Table III.

Overall, the experimental absolutely normalized TDCS are excellently predicted by CCC theory for a large range of kinematics and collision geometries as shown in the Figs. 1–4. The TDCC theory is very accurate in shape and magnitude of the TDCS at equal energy sharing (Fig. 4). Concerning the discrepancies between TDCC and experiments, we note that the equal energy sharing TDCS converge much more rapidly with respect to the number of partial waves included in the calculation compared to the very asymmetric energy sharing. Also, for the very slow electron TDCS, large radial meshes are often required. Although the TDCC calculations presented here appear well converged with respect to both of these parameters, we plan further convergence checks for the most asymmetric energy sharing TDCS. We also plan to test the accuracy of our 'frozen-core' approximation for the non-ionized electron. As discussed in [11], we use a local-exchange potential to describe the interaction of the non-ionized electron with the scattered and ionized electron. We plan to perform three-electron TDCC calculations, which make no such approximations (and can also describe double ionization and ionization-excitation processes) and will enable us to check whether our frozen-core approximation is the cause of the discrepancies found here for very unequal energy sharing

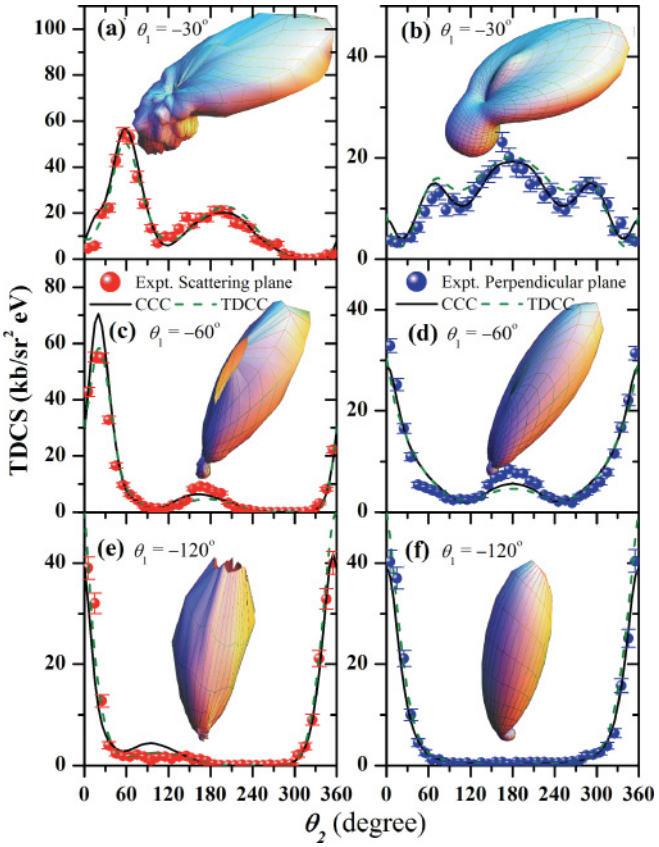


FIG. 4. (Color online) Absolute TDCS in the scattering (left column) and perpendicular plane (right column) for equal energy sharing ($E_1 = E_2 = 23$ eV) as a function of the emission angle of one electron ($\theta_2$) with the other electron's emission angle $\theta_1$ being fixed to (a) and (b) $\theta_1 = -30°$; (c) and (d) $\theta_1 = -60°$; (e) and (f) $\theta_1 = -120°$. The insets in (a)–(f) are the 3D patterns of the TDCS for the experiment (left column) and CCC calculation (right column).

cross sections. Such calculations are quite computationally intensive and will be reported in due course.

## IV. SUMMARY

In summary, we have performed a comprehensive study of single ionization of helium by 70.6-eV electron impact. The experimental cross sections are compared to the predictions of the CCC and the TDCC calculations for a large range of kinematics and collision geometries. The TDCS as 3D patterns show excellent qualitative agreement. Comprehensive quantitative comparisons of experiment and theories are presented in the scattering and perpendicular planes. It is found that the TDCC and CCC calculations are in excellent agreement with the experiment for equal energy sharing. Moreover, all the features observed in the experiment, which cover a major part of the entire three-particle final-state configuration, are completely described by the CCC theory with sufficient accuracy, including the absolute magnitude of the cross section. Therefore, we conclude that the theoretical description of single ionization of helium by electron impact leaving the ion in the ground state can be sufficiently accurate for many practical purposes. The full set of experimental data may be obtained on request from the corresponding author.

## ACKNOWLEDGMENTS

X.R. is grateful for support from DFG Project No. RE 2966/1-1. I.B. and D.V.F. are grateful for the support of the Australian Research Council and the Australian National Computational Infrastructure Facility and its Western Australian node iVEC. The Los Alamos National Laboratory is operated by Los Alamos National Security, LLC for the National Nuclear Security Administration of the US Department of Energy under Contract No. DE-AC5206NA25396. A portion of this work was performed through DOE and NSF grants to Auburn University.

[1] T. N. Resigno, M. Baertschy, W. A. Isaacs, and C. W. McCurdy, Science **286**, 2474 (1999).
[2] J. Colgan and M. S. Pindzola, Phys. Rev. A **74**, 012713 (2006).
[3] I. Bray, Phys. Rev. Lett. **89**, 273201 (2002).
[4] T. Rösel, J. Röder, L. Frost, K. Jung, H. Ehrhardt, S. Jones, and D. H. Madison, Phys. Rev. A **46**, 2539 (1992).
[5] X. Ren *et al.*, Phys. Rev. A **82**, 032712 (2010).
[6] H. Ehrhardt, K. Jung, G. Knoth, and P. Schlemmer, Z. Phys. D **1**, 3 (1986).
[7] A. Murray and F. H. Read, J. Phys. B: At. Mol. Phys. **26**, L359 (1993).
[8] M. Dürr, C. Dimopoulou, B. Najjari, A. Dorn, and J. Ullrich, Phys. Rev. Lett. **96**, 243202 (2006).
[9] L. Avaldi, R. Camilloni, E. Fainelli, G. Stefani, A. Franz, H. Klar, and I. E. McCarthy, J. Phys. B: At. Mol. Phys. **20**, 5827 (1987).
[10] A. Duguet, M. Cherid, A. Lahmam-Bennani, A. Franz, and H. Klar, J. Phys. B: At. Mol. Phys. **20**, 6145 (1987).
[11] J. Colgan, M. S. Pindzola, G. Childers, and M. A. Khakoo, Phys. Rev. A **73**, 042710 (2006).
[12] J. Colgan, M. Foster, M. S. Pindzola, I. Bray, A. T. Stelbovis, and D. V. Fursa, J. Phys. B: At. Mol. Phys. **42**, 145002 (2009).
[13] I. Bray, D. V. Fursa, A. S. Kadyrov, and A. T. Stelbovics, Phys. Rev. A **81**, 062704 (2010).
[14] A. T. Stelbovics, I. Bray, D. V. Fursa, and K. Bartschat, Phys. Rev. A **71**, 052716 (2005).
[15] I. Bray and D. V. Fursa, Phys. Rev. A **54**, 2991 (1996).
[16] J. Ullrich, R. Moshammer, A. Dorn, R. Dörner, L. Ph H Schmidt, and H. Schmidt-Böcking, Rep. Prog. Phys. **66**, 1463 (2003).
[17] M. Dürr, C. Dimopoulou, A. Dorn, B. Najjari, I. Bray, D. V. Fursa, Z. Chen, D. H. Madison, K. Bartschat, and J. Ullrich, J. Phys. B: At. Mol. Phys. **39**, 4097 (2006).
[18] X. Ren, A. Senftleben, T. Pflüger, A. Dorn, K. Bartschat, and J. Ullrich, J. Phys. B: At. Mol. Phys. **43**, 035202 (2010).
[19] I. Bray, D. V. Fursa, J. Röder, and H. Ehrhardt, J. Phys. B: At. Mol. Phys. **30**, L101 (1997).
[20] M. Schulz, R. Moshammer, D. Fischer, H. Kollmus, D. H. Madison, S. Jones, and J. Ullrich, Nature (London) **422**, 48 (2003).
[21] O. Al-Hagan, C. Kaiser, D. Madison, and A. J. Murray, Nat. Phys. **5**, 59 (2009).